Clinical Biomechanics 80 (2020) 105138

Contents lists available at ScienceDirect

Clinical Biomechanics

journal homepage: www.elsevier.com/locate/clinbiomech

In silico optimization of targeted aerosol delivery in upper airways via Inhaled Volume Tracking

Metar Heller-Algazi[a], Eliram Nof[a], Prashant Das[b], Saurabh Bhardwaj[a], Stavros C. Kassinos[c], Josué Sznitman[a,*]

[a] Department of Biomedical Engineering, Technion – Israel Institute of Technology, Haifa 3200003, Israel
[b] Department of Mechanical Engineering, University of Alberta, Alberta, Canada
[c] Computational Sciences Laboratory (UCY-CompSci), Department of Mechanical and Manufacturing Engineering, University of Cyprus, Kallipoleos Avenue 75, Nicosia 1678, Cyprus

ARTICLE INFO

Keywords:
Inhalation therapy
In silico
Aerosol deposition
Drug delivery
Computational fluid dynamics
Lungs

ABSTRACT

Background: Despite the widespread use of aerosol inhalation as a drug delivery method, targeted delivery to the upper airways remains an ongoing challenge in the quest for improved clinical response in respiratory disease.
Methods: Here, we examine *in silico* flow and particle dynamics when using an oral Inhaled Volume Tracking manoeuvre. A short pulsed aerosol bolus is injected during slow inhalation flow rates followed by clean air, and a breath-hold is initiated once it reaches the desired depth. We explore the fate of a broad particle size range (1–40 μm) for both upright and supine positions.
Findings: Our findings illustrate that despite attempts to mitigate dispersion using slower flow rates, the laryngeal jet disperses the aerosol bolus and thus remains a hurdle for efficient targeted delivery. Nevertheless, we show a decrease in extra-thoracic deposition; large aerosols in the range of 10–30 μm potentially outperform existing inhalation methods, showing deposition fractions of up to 80% in an upright orientation.
Interpretation: The improved deposition during Inhaled Volume Tracking shows promise for clinical applications and could be leveraged to deliver larger payloads to the upper airways.

1. Introduction

Inhalation therapy represents the most common treatment modality for respiratory diseases, in particular for asthma, one of the most prevalent chronic disorders worldwide (Asher and Pearce, 2014; Beasley et al., 2000; Lundbäck et al., 2016). When compared to oral administration, aerosol inhalation is frequently preferred due to rapid drug uptake as well as reduction in dosage requirements and corresponding side effects (Patton and Byron, 2007; Sakagami, 2006). However, treatment efficacy is greatly dependent on the drugs reaching their target site (Pleasants and Hess, 2018). In the case of asthma and constrictive airway diseases for example, targeting the conductive airways (e.g. large to small bronchi) is desirable (Ebina et al., 1990). In practice, yet, only a small fraction of the inhaled dose (i.e. estimated between 15–40% in adults (Delvadia et al., 2012; Wei et al., 2018)) deposits in the lungs with the rest lost to both the inhaler and the extrathoracic airways (i.e. mouth-throat region). More dramatically, an even smaller fraction (i.e. < 1% for the smaller bronchial airways) reaches the intended site (Longest et al., 2019). In turn, loss of the bulk dose can have deleterious effects as aerosols deposit in undesirable regions or may instead require an increase in dosage to reach the therapeutic concentration at the initially intended target site (Kleinstreuer et al., 2008; Koullapis et al., 2018).

A key to efficient local or regional pulmonary targeting lies for example in minimizing particle dispersion (Darquenne, 2012); a challenge that has proven difficult to tackle in the conductive airways and in particular in the laryngeal region due to a strong jet that arises (Chan et al., 1980; Lin et al., 2007; Schlesinger and Lippmann, 1976). Inhalation airflows in these regions exhibit complex structures, e.g. turbulence and shear flows, which increase aerosol bolus dispersion (Kleinstreuer and Zhang, 2003; Zhang et al., 2002). This problem is further exacerbated when using inhalation devices that rely on high-velocity flows in order to aerosolize particles for delivery (e.g. dry powder inhalers). In turn, this increases turbulence and aerosol impaction leading to loss of particles to the trachea and extra-thoracic region (Kleinstreuer and Zhang, 2003; Longest et al., 2008). Hence, to maximize regional targeting in the upper bronchial regions, delivery using slower inhalation flow rates which maintain laminar airflows

* Corresponding author.
E-mail address: sznitman@bm.technion.ac.il (J. Sznitman).

https://doi.org/10.1016/j.clinbiomech.2020.105138
Received 4 March 2020; Accepted 28 July 2020
0268-0033/

would therefore be desirable; a point that has been previously acknowledged e.g. in the development of the soft mist inhaler which produces slower-moving aerosol jets (Dalby et al., 2004; Hochrainer et al., 2005). Various strategies have thus been put forward to improve aerosol targeting of specific lung regions. For example, selecting specific particle sizes has been shown to improve aerosol deposition in the upper airways where aerosols within the narrow range of 2–6 μm are considered best for tracheobronchial deposition (Darquenne, 2012; Negro, 2015; Usmani et al., 2005). Yet, only a small fraction of the total inhaled dose is nevertheless delivered to the upper bronchial region, with the rest exhaled or deposited in more distal regions (Bailey, 1994; Heyder et al., 1986). Recent work has expanded the concept of tailoring particle size as a function of the choice of inhalation manoeuvre and patient age group (Das et al., 2018). However, continuous inhalation of particles, as in the case of nebulizers, still limits deposition affinity as aerosols are indiscriminately spread across broad regions of the lungs.

To improve localized aerosol deposition, an Inhaled Volume Tracking (IVT) method has been recently proposed that circumvents the limitations of continuous inhalation of nebulized suspensions while minimizing impaction losses with DPI (Ostrovski et al., 2019). Briefly, this method involves the injection of a short pulsed, compact bolus of (e.g. nebulized) aerosols into a slow, steady inhaled airflow followed by clean air behind the aerosol bolus. Once a specific clean air volume (CAV) is calibrated for the particle bolus to reach the desired depth of the target site, a short breath-hold manoeuvre is implemented to facilitate deposition via particle sedimentation. This technique allows for relative improvement of deposition within a confined region of airways. While the IVT manoeuvre shows promise for more accurate generational targeting in achieving a more confined lung deposition region, it has so far only been examined for scenarios involving intubated lungs using an endotracheal tube that circumvents altogether the existence of particle dispersion due to the laryngeal jet (Lin et al., 2007). For mild or chronic respiratory disorders, clinical intubation is not a viable treatment option and less invasive options are sought (e.g. home use) when considering common inhalation therapy.

Motivated by the ongoing need to improve selected deposition of aerosols to target lung regions for efficient inhalation therapy for conductive airway diseases (e.g. asthma), here we explore *in silico* the opportunity of IVT as a non-invasive strategy that has the potential for general clinical use in inhalation therapy. Using an anatomically-realistic model of adult human airways, we implement an IVT inhalation manoeuvre and simulate inhaled aerosols spanning a broad range of clinically-relevant particle sizes, as well as particles hitherto considered too large for traditional inhalation manoeuvres using DPI. We exemplify here the case of a fixed CAV value for upper airway targeting and show that while slower flow rates in the laminar regime cannot circumvent mixing due to the intrinsic existence of the laryngeal jet, our method supports the notion of improved upper airway deposition over traditional inhalation approaches. Namely, we identify a window of large micron particle sizes optimally suited for such manoeuvre. We further characterize how inhalation position (upright vs. supine) strongly affects targeting outcomes. Finally, we discuss the practical implications and limitations of this inhalation technique for broader clinical applications.

2. Methods

2.1. Airway model

We simulate aerosol transport and deposition from mouth to upper airways under the IVT method. Our selected geometry comprises a morphometrically-faithful model of the human upper airways of an adult male, previously used in aerosol deposition simulations (Das et al., 2018). Briefly, it consists of an idealized model of the extra-thoracic (i.e mouth-throat, MT) region validated by Xi and Longest (2007) coupled to a tracheo-bronchial tree which follows the morphometric model of Horsfield et al. (1971) and Weibel et al. (1963), featuring a seven-generation tree of asymmetric, dichotomous branching airways. The complete airway model is presented in Fig. 1A. The geometry is divided into three regions (i.e. mouth-throat, trachea and conducting airways) to facilitate quantification of deposition patterns (see Section 3) and holds 64 distal outlets grouped by their respective lobar region (i.e. Right-Upper, Right-Middle, etc).

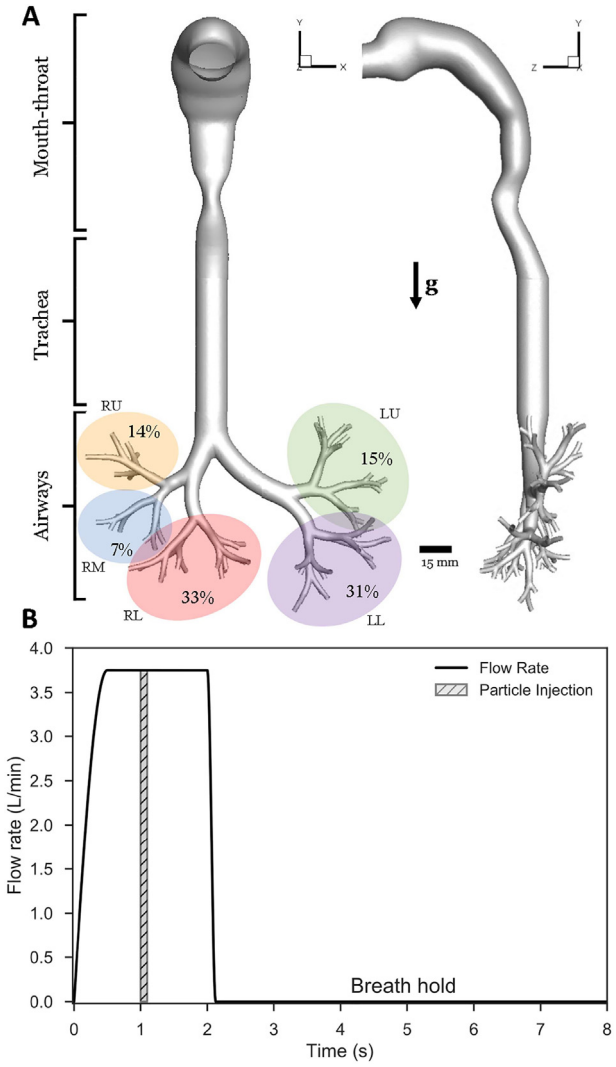

Fig. 1. (A) Computer-aided drawing (CAD) of the upper airway anatomy spanning the extra-thoracic airways (i.e. mouth-throat) down to the 6th generation of the conductive region. The various lobes of the lungs (e.g. upper/middle/bottom right lobe; upper/lower left lobe) are color-coded and identified according to the percentage of ventilation distribution across the lungs. (B) Profile of the inhalation manoeuvre (i.e. flow rate) over time, illustrating the particle injection period and the breath hold duration.

2.2. Inhalation manoeuvre

An IVT inhalation manoeuvre has been recently implemented (Ostrovski et al., 2019), with a characteristic profile shown in Fig. 1B. A peak inspiratory flow rate (PIFR) of 3.75l min^{-1} ensures that the peak Reynolds number (defined as $Re = uL/\nu$ where u is the characteristic velocity of air, L the characteristic length and ν the kinematic viscosity) in the laryngeal region remains approximately ~500. Even under normal inhalation conditions (15l min^{-1}), the local Reynolds number in the laryngeal region can reach above 1250 (Kleinstreuer and Zhang, 2003), typically giving rise to transitional flow characteristics that may

lead to strong aerosol dispersion (Das et al., 2018; Koullapis et al., 2018). Here, rather our strategy aims to minimize such effects while maintaining a clinically-realizable inhalation flowrate. Specifically, we explore a total inhalation time set at 2 s and a fixed CAV of 62.5 ml (1 s of inhalation after bolus injection), corresponding to the total airway volume proximal to the first bifurcation. Such approch displaces the entire aerosol bolus into the entrance of the upper airways. Following that, a 6 s breath hold is implemented to allow for particle deposition under the action of sedimentation only. Note that the gravitational force is aligned downwards simulating an upright patient, while a supine alignment is explored for comparison (see Supplementary material).

2.3. Numerical simulations

Numerical simulations of the respiratory inhalation manoeuvre (Fig. 1B) are performed using a commercial CFD software (Fluent 17.2, ANSYS, Inc). Briefly, the conservation of mass and momentum (i.e Navier-Stokes) equations for air are solved using the Finite Volume Method (FVM). To generate the computational mesh, the geometry was first divided into tetrahedral elements using ICEM (ANSYS, Inc). The generated mesh was refined and subsequently imported into Fluent for conversion to polyhedral cells which offer improved computational performance (Sosnowski et al., 2017). Prism layers of varying thickness were implemented at the wall to ensure accurate resolution of near-wall flows critical to deposition. Mesh convergence tests covering 2 M to 6 M tetrahedral cells ensured errors for centreline velocity profiles and secondary flow streamlines along key locations (e.g. along the trachea and bronchi) remain < 2% compared to the finest mesh explored. The final mesh selected was 0.9 M polyhedral elements in size, down from 2.4 M tetrahedral elements, with a maximum of 10 prism layers near critical wall regions.

Flow rate at the inlet is set using a velocity inlet boundary condition, imposing a uniform velocity along the entire surface (i.e. mouth). Airway walls are modelled as rigid, absorbing (i.e particles cannot escape once deposited) boundaries with a no-slip condition. Model outlets are divided into five groups according to their downstream lung lobe ventilation fraction following physiological estimates (Fig. 1A), with 14% of outflow going to the right upper (RU) lobe, 7% to the right middle (RM), 33% to the right lower (RL), 15% to the left upper (LU) and 31% to the left lower (LL) lobes, respectively (Walenga et al., 2013). Corresponding outflows are weighed using a fractional flow rate boundary condition. A laminar solver was used with a coupled pressure-velocity scheme along with a Least-Squares based scheme for gradients and a 2nd Order Upwind scheme for both velocity and pressure terms. For the transient term, a second-order implicit scheme was implemented with a time-step size of 10^{-3} s; see further details in recent studies (Bauer et al., 2019; Das et al., 2018).

2.4. Aerosol transport

Computation of aerosol particle motion and deposition was implemented using a Lagrangian-based, one-way coupled discrete phase model, under the assumption that particles are disperse enough not to interact with one another nor influence the flow field (Finlay, 2001). Forces governing particle motion are assumed to be viscous Stokes drag and gravitational sedimentation, while displacements due to Brownian motion may be safely neglected for particles $\geq 1\,\mu$m in size (Hofemeier and Sznitman, 2015). Here, we neglect the effects of electrostatic forces or hygroscopic growth (Koullapis et al., 2016).

Spherical particles ($\rho = 1000\,\mathrm{kg/m^3}$) were injected at the mouth inlet surface using a uniform random distribution; for each size run, roughly 28′500 particles were seeded to ensure deposition fractions independent of particle number (Das et al., 2018). Particle diameters span the range of 1–40 μm in diameter (1–15 μm in the upright case). Particles were tracked until either depositing at a wall or exiting through one of the outlets and assumed deposited in the lower airways, as this study is limited to deposition in the upper conductive airways.

2.5. Experimental flow visualization

To compare our numerical airflow solutions, the three-dimensional (3D) velocity fields were experimentally investigated under laminar flow conditions using a high-speed, tomographic particle image velocimetry (tomoPIV) technique on a transparent, silicone, mouth-throat phantom which was cast from the same CAD geometry used in the numerical study. Briefly, tomoPIV uses multiple (3 +) cameras to track the movement of fluorescent tracer particles suspended in a fluid flowing in 3D space. Using an Eulerian approach, images are processed to identify groups of particles with cross-correlation algorithms applied between subsequent frames in time to extract the 3D velocity vectors. Note that PIV relies on statistical tracking of seeded particles which limits resolution near wall regions (i.e. where particle density is low) (Nof et al., 2020; Westerweel et al., 2013). To match mean Re values in experiments, the model was scaled down homothetically by a factor of approximately 2 to account for differences in working fluids (i.e. air and a 58% glycerol-water solution). The imaging acquisition rate used was 1′000 frames per second with a final vector density of 0.2 mm. Details on the extensive methodology can be found in the recent work by Nof et al. (2020).

3. Results & discussion

3.1. Airflow patterns in IVT

To first gain insight into the respiratory flow patterns underlying aerosol transport during the IVT inhalation manoeuvre, Fig. 2A shows velocity magnitude $|\mathbf{u}|$ contours during stable peak inhalation just prior to the onset of particle injection (i.e. $t = 1$ s); this is shown at an inspiratory flow rate of $3.75\,\mathrm{l\,min^{-1}}$, when flow fields are at peak strength. Results are shown for the coronal and sagittal axes along the tracheal centreline, bisecting the mouth-throat and trachea regions as well as the first two bronchial bifurcations, respectively. The peak instantaneous Reynolds number is approximately Re ~ 530 at the larynx where flows are fastest, while flow remains laminar throughout the airways. Despite significantly slower velocity magnitudes ($|\mathbf{u}|_{\max} \approx 1\,\mathrm{m\,s^{-1}}$), underlying flow structures visible in the contour plots remain largely comparable to those previously reported for DPI and other high-velocity inhalation manoeuvres (Das et al., 2018; Xi and Longest, 2007). Notably, flow accelerates at the larynx to form the characteristic laryngeal jet; a hallmark feature of respiratory inhalation flows and shown to play a role in aerosol deposition (Xi et al., 2008). This jet is tied to the intrinsic anatomical structure, brought upon by a coupling of local constriction and curvature (Koullapis et al., 2018). Shear flows amplified by the laryngeal jet produce stark differences in penetration depths of inhaled aerosols, visible in the accompanying Supplementary video 1 depicting particle trajectories during an IVT manoeuvre (i.e. particles travelling along a high-velocity streamline penetrate deeper into the airways compared with particles moving in a region of slower flow). Moreover, these rapid changes in direction of high-velocity flows are known to cause aerosol impaction on the airway walls (Cheng et al., 1999). Flow fields obtained from tomoPIV experiments (see Fig. 2A inset) further support our *in silico* results, underlining the persistent occurrence of a laryngeal jet even under laminar conditions.

We briefly continue our flow analysis comparing secondary flow fields along cross-sections, as shown in Fig. 2B. Here, velocity magnitude contours of spanwise cross-sections at the larynx (I), upper and lower trachea (II and III, respectively) are overlaid with secondary flow streamlines (left column). As flow exits the trachea downstream, symmetric vortices are apparent which transfer particles within streamlines. Further down the trachea, these vortices dissipate and flow

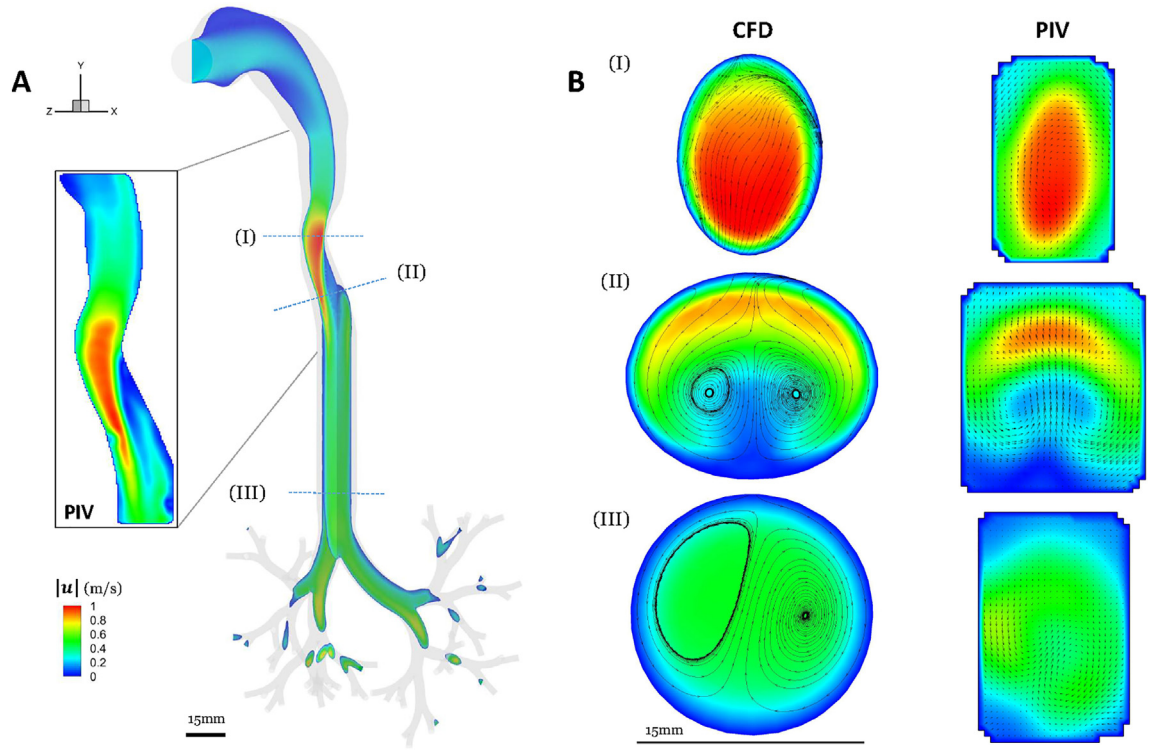

Fig. 2. (A) Contours of the instantaneous velocity magnitude ($|\mathbf{u}|$) along the sagittal (y-z) and coronal (x-y) planes shown at peak inhalation flow rate. Inset shows velocity magnitude field from experimental tomoPIV. (B) Corresponding velocity magnitude contours along selected cross-sections as shown in (A) along along with secondary flow streamlines for CFD (left) and tomoPIV (right).

gradually returns to a more fully developed, Poiseuille-like profile (Fig. 2A). *In silico* results are compared to matching cross-sections obtained from tomo PIV (right column); key flow elements (i.e. velocity magnitudes, vortex structures) compare well with the computational results. Similar to axial flow, patterns of secondary flows appear qualitatively similar to those previously reported for higher Re (Das et al., 2018; Xi and Longest, 2007); this suggests that by and large, despite significantly reduced velocities (and a corresponding decrease in Reynolds number) throughout the lungs, qualitative flow features in IVT inhalation exhibit similar characteristics to those reported for faster manoeuvres such as DPI inhalations. Therefore, even though turbulent flow characteristics are mitigated, other dispersive features (e.g. shear flow, vortex structures) remain present during the inhalation manoeuvre and are anticipated to contribute to aerosol dispersion (see below).

3.2. Aerosol deposition outcomes

To assess aerosol deposition outcomes following the IVT manoeuvre, we first exemplify deposition patterns in an upright position in Fig. 3 for three representative particle sizes, namely 3, 12 and 25 μm; particles are color-coded according to deposition density normalized by the highest density observed for comparison purposes across sizes. Other particle sizes are provided in Supplementary Fig. 1. While regional variations in deposition densities are observed (consider the deposition of 12 μm compared to 25 μm particles in Fig. 3), higher deposition is centred in the first bifurcations of the bronchi, except for very large particles (> 25 μm) which deposit preferentially in the extrathoracic region. Note that the distribution between branches is heterogeneous, with some showing little, if any, aerosol deposition (e.g. in the upper- and middle-right lobe).

We recall that impaction phenomena are captured by the dimensionless Stokes number. Briefly, the Stokes number describes the relative importance of inertia on particle trajectory, and is defined as (Darquenne, 2012; Hofemeier and Sznitman, 2015):

$$\mathrm{Stk} = \frac{\rho_p d_p^2 \, |\mathbf{u}| \, C_c}{18 \mu D_0},$$

where ρ_p and d_p are the respective particle density and diameter; $|\mathbf{u}|$ and μ the velocity and dynamic viscosity of the fluid (i.e. air); C_c the Cunningham slip correction factor and D_0 a characteristic length scale (i.e. mouth hydraulic diameter). Here, we calculate Stk using the velocity and hydraulic diameter at the mouth inlet. Stokes numbers for aerosols simulated here range from $\mathrm{Stk} \sim e-4$ for the smallest particles (i.e. 1–3 μm) to $\mathrm{Stk} \sim e-1$ for the largest particles (i.e. 30–40 μm). Here, we observe that smaller aerosols (i.e. $\mathrm{Stk} \ll 1$) follow streamlines well as inertial forces are negligible, whereas as Stk increases the effects of inertia are more apparent, evidenced by changes in locations of peak deposition and ultimately an increase in extrathoracic deposition due to impaction. Correspondingly, sedimentation is dependent on the terminal settling velocity of the particles (Darquenne, 2012; Sznitman, 2013), where for aerosols > 5 μm in size complete deposition can be expected during the breath hold duration for particles in the upper airways.

We quantify deposition fractions for each particle size defined as the ratio between deposited aerosols in each region to the total inhaled aerosol bolus, shown for an upright patient in Fig. 4A. Note that "lower airways" correspond to aerosols that have exited the 64 outlets of the computational model. Peak deposition efficiency in the upper airways is observed for aerosols spanning 10–30 μm in size, with up to 80% of the inhaled fraction ending up at the initially targeted site. In comparison, typical *in vitro* assessment of current DPI inhalers suggests deposition fractions closer to 20% or less (Bailey, 1994; Delvadia et al., 2012), thus supporting an opportunity for significant improvement. Upper airway deposition increases with aerosol particle size, as smaller aerosols (1–5 μm) show lower deposition fractions when compared to larger aerosols (> 7 μm); the lower sedimentation rate of small aerosols leaves more particles in suspension. The deposition fraction in the mouth-

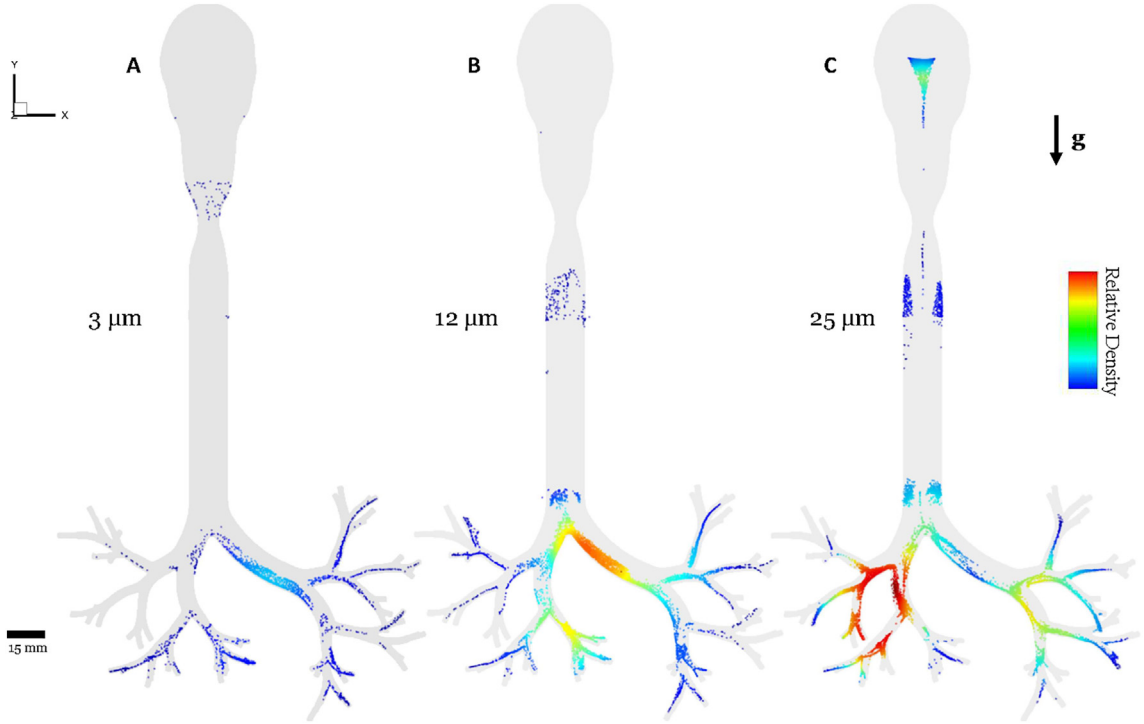

Fig. 3. Aerosol deposition maps following an IVT inhalation manoeuvre in an upright position for selected particle sizes. Color-coding corresponds to the relative density of particles deposited on the airways; peak density is at the 2nd generation of the right lobe, for 25.

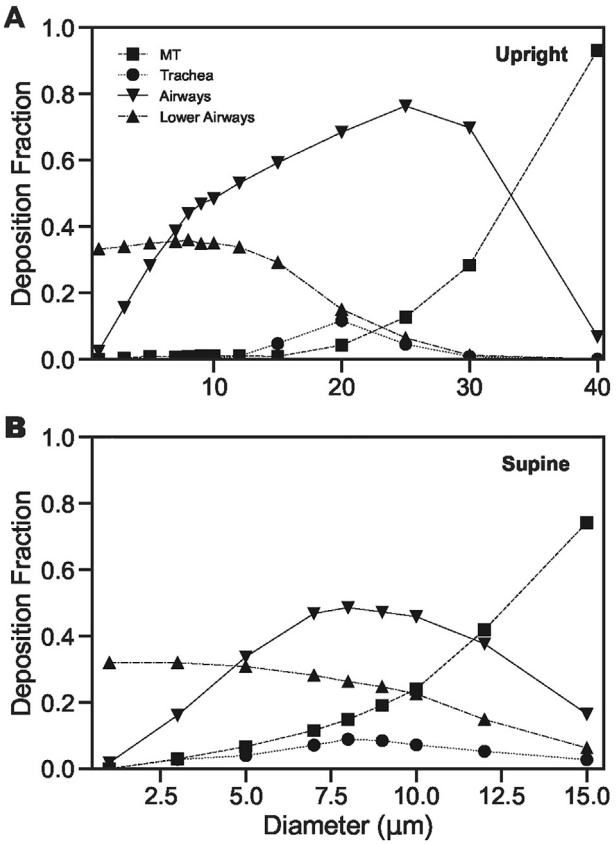

Fig. 4. Summary of aerosol deposition fractions for upright (A) and supine (B) positions according to the defined lung regions of Fig. 1A.

throat region is negligible for aerosols < 15 μm in size where Stk < 10^{-2}. Meanwhile, the fraction inhaled deeply into the lower airways remains relatively constant around 30% for these particle sizes, underscoring that impaction is negligible where Stk < 10^{-2}. Deposition in the mouth-throat region rises to become the largest fraction for very large aerosols (i.e. 40 μm, Stk = 0.067) which predominantly impact the back of the mouth-throat (MT) area, posing a practical size limit for inhalation aerosols using IVT. Such results stand in contrast to MT deposition fractions for DPI inhalers, which are closer to 50–70% already for ~2 μm aerosols (Longest et al., 2012; Wei et al., 2018). An optimal window for aerosol delivery, therefore, appears to be in the range of 10–30 μm sized particles, balancing the trade-off between sedimentation rate, extra-thoracic deposition and deep-airway penetration. This range spans aerosol sizes 2–4 times larger than common inhalation aerosols. Notably, due to the decrease in flow rate, Stokes numbers for these aerosols (Stk = 0.01 − 0.03) are in line with reports for nebulized inhalation (Das et al., 2018). The IVT technique thus allows in principle to leverage these larger sized aerosols that would otherwise be lost to impaction with traditional nebulized or DPI approaches, giving opportunity for larger payloads.

When considering a supine orientation, particle deposition patterns differ significantly (see Fig. 4B). Here, extra-thoracic deposition becomes prevalent already for smaller aerosol particles > 5 μm in size, resulting in lower peak deposition density as more particles are lost to impaction; consider that extra-thoracic deposition is negligible in an upright orientation for aerosols < 15 μm in diameter. Whereas in absence of other forces particles sediment down the trachea in an upright patient, for a supine alignment particles will sediment at the depth they reach when breath-hold is initiated, further increasing deposition in the trachea and mouth-throat regions. While the fraction of aerosols inhaled into the deeper airways remains similar to the upright case at around 30%, upper airway deposition shows a shift in optimal sizing with peak upper airway deposition efficiency of approximately 50% seen in particles 7–10 μm in size (compared to 10–30 μm in an upright orientation). The drop-off in upper airway deposition (coupled with a rise in extra-thoracic deposition) occurs already for 12–15 μm sized

particles. Notably, however, for no particle size does the upper airway fraction reach the deposition fractions seen for an upright patient, with a peak of only 50% compared to 80% between the two cases.

3.3. Limitations

In the present work, a short, compact bolus can be viewed as analogous to an "impulse response" in the airway tree to an inhalation manoeuvre by sampling many deterministic trajectories; the resulting deposition patterns are then similar to a probability density function of particle deposition. Although particles were injected for a fixed short pulsed 0.1 s bolus, deposition maps show a wide spread of particles throughout the airways. This stands in contrast to past studies on intubated patients where the aerosol bolus remains more compact (Ostrovski et al., 2019), recalling that an endotracheal tube bypasses the larynx, thus entirely avoiding effects of the laryngeal jet. Such intrinsic scattering will have profound effects on targeting accuracy as aerosols span the entire length of the upper airways, from trachea to the distal airways. Such outcomes underscore the importance of the laryngeal jet as a defining feature of respiratory flows in the upper airways and its repercussions on inhalation therapy outcomes.

We briefly note that the uneven distribution of deposited aerosols between airway branches is foreseeably linked to regional flow rate distribution (Darquenne et al., 2011). This could prove challenging in the treatment of restrictive respiratory disorders as the target region would receive a reduced drug dose due to restricted, or at the very least altered, flow rate (Darquenne, 2012). In this study, an idealized rigid airway model was used with outlet flow rate weighting typical of healthy lungs; patient-specific models that include airway narrowing or other diseased features would possibly bias deposition patterns, as shown e.g. for cystic fibrosis patients (Anderson et al., 1989; Darquenne, 2012). Despite such *in silico* limitations, the underlying premise of an IVT approach supports the opportunity to leverage a short pulsed bolus of large sized aerosols for relative improvement of local deposition.

4. Conclusions

Improving the deposition efficiency of inhaled aerosols is an imperative in the treatment of respiratory diseases. Here, we explored *in silico* the prospects of the IVT technique in achieving this goal not only for intubated patients but also for oral inhalation. In this study, we exemplify improved deposition using our proposed manoeuvre compared to typical other inhalation methods, but also pinpoint some general characteristics inherent to oral inhalation in particular, in the presence of the laryngeal jet even under laminar conditions.

Despite these limitations, our results support the notion of a dramatic improvement in upper-airway deposition efficiency over traditional inhalation methods for a range of aerosol particle diameters, with deposited fractions up to 80% of the total inhaled dose. The IVT manoeuvre is found to be significantly more effective when the patient is oriented upright compared to a supine position, showing both higher upper airway deposition fractions as well as reduction in extra-thoracic deposition. Moreover, lower airflow velocities required for this manoeuvre not only enable, but call for, use of particle sizes larger than hitherto used for inhalation treatment. We observe a broad window of particle sizes between 10 and 30 μm that provide the best results in terms of deposition efficiency opening up an opportunity for larger aerosol particles than previously considered, with a bigger therapeutic payload per particle. Finally, although an inhaler required to deliver a pulsed aerosol bolus could increase cost and complexity, the manoeuvre could promise improved drug delivery to the target side with a reduction of superfluous deposition elsewhere.

Supplementary data to this article can be found online at https://doi.org/10.1016/j.clinbiomech.2020.105138.

Declaration of Competing Interest

None.

Acknowledgements

This work was supported by the European Research Council (ERC) under the European Unions Horizon 2020 research and innovation program (grant agreement No. 677772). The authors acknowledge COST Action MP1404 SimInhale 'Simulation and pharmaceutical technologies for advanced patient-tailored inhaled medicines', supported by the European Cooperation in Science and Technology (COST).

References

Anderson, P.J., Blanchard, J.D., Brain, J.D., Feldman, H.A., Mcnamara, J.J., Heyder, J., 1989. Effect of cystic fibrosis on inhaled aerosol boluses. Am. Rev. Respir. Dis. 140 (5), 1317–1324.
Asher, I., Pearce, N., 2014. Global burden of asthma among children. Int. J. Tuberc. Lung Dis. 18 (11), 1269–1278.
Bailey, M.R., 1994. The new ICRP model for the respiratory tract. Radiat. Prot. Dosim. 53 (1–4), 107–114.
Bauer, K., Nof, E., Sznitman, J., 2019. Revisiting high-frequency oscillatory ventilation in vitro and in silico in neonatal conductive airways. Clin. Biomech. 66, 50–59.
Beasley, R., Crane, J., Lai, C.K., Pearce, N., 2000. Prevalence and etiology of asthma. J. Allergy Clin. Immunol. 105 (2), S466–S472.
Chan, T.L., Schreck, R.M., Lippmann, M., 1980. Effect of the laryngeal jet on particle deposition in the human trachea and upper bronchial airways. J. Aerosol Sci. 11 (5), 447–459.
Cheng, Y.-S., Zhou, Y., Chen, B.T., 1999. Particle deposition in a cast of human oral airways. Aerosol Sci. Technol. 31 (4), 286–300.
Dalby, R., Spallek, M., Voshaar, T., 2004. A review of the development of Respimat® Soft Mist Inhaler. Int. J. Pharm. 283 (1), 1–9.
Darquenne, C., June 2012. Aerosol deposition in health and disease. J. Aerosol Med. Pulm. Drug Deliv. 25 (3), 140–147.
C. Darquenne, C. van Ertbruggen, and G. K. Prisk. Convective flow dominates aerosol delivery to the lung segments. J. Appl. Physiol., 111(1):48–54, 2011.
Das, P., Nof, E., Amirav, I., Kassinos, S.C., Sznitman, J., 2018. Targeting inhaled aerosol delivery to upper airways in children: insight from computational fluid dynamics (CFD). PLoS One 13 (11), e0207711.
Delvadia, R., Hindle, M., Longest, P.W., Byron, P.R., 2012. In vitro tests for aerosol deposition II: IVIVCs for different dry powder inhalers in normal adults. J. Aerosol Med. Pulm. Drug Deliv. 26 (3), 138–144.
Ebina, M., Yaegashi, H., Chiba, R., Takahashi, T., Motomiya, M., Tanemura, M., 1990. Hyperreactive site in the airway tree of asthmatic patients revealed by thickening of bronchial muscles: a morphometric study. Am. Rev. Respir. Dis. 141 (5_pt_1), 1327–1332.
Finlay, W.H., 2001. The Mechanics of Inhaled Pharmaceutical Aerosols: An Introduction. Academic Press.
Heyder, J., Gebhart, J., Rudolf, G., Schiller, C.F., Stahlhofen, W., 1986. Deposition of particles in the human respiratory tract in the size range 0.005–15 Mm. J. Aerosol Sci. 17 (5), 811–825.
Hochrainer, D., Hölz, H., Kreher, C., Scaffidi, L., Spallek, M., Wachtel, H., 2005. Comparison of the aerosol velocity and spray duration of Respimat® Soft Mist™ Inhaler and pressurized metered dose inhalers. J. Aerosol Med. 18 (3), 273–282.
Hofemeier, P., Sznitman, J., 2015. Revisiting pulmonary acinar particle transport: convection, sedimentation, diffusion, and their interplay. J. Appl. Physiol. 118 (11), 1375–1385.
Horsfield, K., Dart, G., Olson, D.E., Filley, G.F., Cumming, G., 1971. Models of the human bronchial tree. J. Appl. Physiol. 31 (2), 207–217.
Kleinstreuer, C., Zhang, Z., 2003. Laminar-to-turbulent fluid-particle flows in a human airway model. Int. J. Multiphase Flow 29 (2), 271–289.
Kleinstreuer, C., Zhang, Z., Donohue, J.F., 2008. Targeted drug-aerosol delivery in the human respiratory system. Annu. Rev. Biomed. Eng. 10 (1), 195–220.
Koullapis, P., Kassinos, S.C., Muela, J., Perez-Segarra, C., Rigola, J., Lehmkuhl, O., Cui, Y., Sommerfeld, M., Elcner, J., Jicha, M., Saveljic, I., Filipovic, N., Lizal, F., Nicolaou, L., 2018. Regional aerosol deposition in the human airways: the SimInhale benchmark case and a critical assessment of in silico methods. Eur. J. Pharm. Sci. 113, 77–94.
Koullapis, P.G., Kassinos, S.C., Bivolarova, M.P., Melikov, A.K., 2016. Particle deposition in a realistic geometry of the human conducting airways: effects of inlet velocity profile, inhalation flowrate and electrostatic charge. J. Biomech. 49 (11), 2201–2212.
Lin, C.-L., Tawhai, M.H., McLennan, G., Hoffman, E.A., 2007. Characteristics of the turbulent laryngeal jet and its effect on airflow in the human intra-thoracic airways. Respir. Physiol. Neurobiol. 157 (2), 295–309.
Longest, P.W., Hindle, M., Choudhuri, S.D., Xi, J., 2008. Comparison of ambient and spray aerosol deposition in a standard induction port and more realistic mouth–throat geometry. J. Aerosol Sci. 39 (7), 572–591.
Longest, P.W., Tian, G., Walenga, R.L., Hindle, M., 2012. Comparing MDI and DPI aerosol deposition using in vitro experiments and a new stochastic individual path (SIP)

model of the conducting airways. Pharm. Res. 29 (6), 1670–1688.
Longest, P.W., Bass, K., Dutta, R., Rani, V., Thomas, M.L., El-Achwah, A., Hindle, M., 2019. Use of computational fluid dynamics deposition modeling in respiratory drug delivery. Expert Opin. Drug Deliv. 16 (1), 7–26.
Lundbäck, B., Backman, H., Lötvall, J., Rönmark, E., January 2016. Is asthma prevalence still increasing? Expert Rev. Respir. Med. 10 (1), 39–51.
Negro, R.W.D., 2015. Dry powder inhalers and the right things to remember: a concept review. Multidiscip. Respir. Med. 10 (1), 13.
Nof, E., Heller-Algazi, M., Coletti, F., Waisman, D., Sznitman, J., 2020. Ventilation-induced jet suggests biotrauma in reconstructed airways of the intubated neonate. J. R. Soc. Interface 17 (162), 20190516.
Ostrovski, Y., Dorfman, S., Mezhericher, M., Kassinos, S., Sznitman, J., 2019. Targeted drug delivery to upper airways using a pulsed aerosol bolus and Inhaled Volume Tracking method. Flow Turbul. Combust. 102 (1), 73–87.
Patton, J.S., Byron, P.R., 2007. Inhaling medicines: delivering drugs to the body through the lungs. Nat. Rev. Drug Discov. 6 (1), 67–74.
Pleasants, R.A., Hess, D.R., 2018. Aerosol delivery devices for obstructive lung diseases. Respir. Care 63 (6), 708–733.
Sakagami, M., 2006. In vivo, in vitro and ex vivo models to assess pulmonary absorption and disposition of inhaled therapeutics for systemic delivery. Adv. Drug Deliv. Rev. 58 (9), 1030–1060.
Schlesinger, R.B., Lippmann, M., 1976. Particle deposition in the trachea: in vivo and in hollow casts. Thorax 31 (6), 678–684.
Sosnowski, M., Krzywanski, J., Gnatowska, R., 2017. Polyhedral meshing as an innovative approach to computational domain discretization of a cyclone in a fluidized bed CLC unit. E3S Web Conf. 14:01027.
Sznitman, J., 2013. Respiratory microflows in the pulmonary acinus. J. Biomech. 46 (2), 284–298.
Usmani, O.S., Biddiscombe, M.F., Barnes, P.J., 2005. Regional lung deposition and bronchodilator response as a function of *B*2-agonist particle size. Am. J. Respir. Crit. Care Med. 172 (12), 1497–1504.
Walenga, R.L., Tian, G., Longest, P.W., 2013. Development of characteristic upper tracheobronchial airway models for testing pharmaceutical aerosol delivery. J. Biomech. Eng. 135 (9).
Wei, X., Hindle, M., Kaviratna, A., Huynh, B.K., Delvadia, R.R., Sandell, D., Byron, P.R., 2018. In vitro tests for aerosol deposition. VI: realistic testing with different mouth–throat models and in vitro—in vivo correlations for a dry powder inhaler, metered dose inhaler, and soft mist inhaler. J. Aerosol Med. Pulm. Drug Deliv. 31 (6), 358–371.
Weibel, E.R., Cournand, A.F., Richards, D.W., 1963. Morphometry of the Human Lung. vol. 1 Springer.
Westerweel, J., Elsinga, G.E., Adrian, R.J., 2013. Particle image velocimetry for complex and turbulent flows. Annu. Rev. Fluid Mech. 45 (1), 409–436.
Xi, J., Longest, P.W., 2007. Transport and deposition of micro-aerosols in realistic and simplified models of the oral airway. Ann. Biomed. Eng. 35 (4), 560–581.
Xi, J., Longest, P.W., Martonen, T.B., 2008. Effects of the laryngeal jet on nano- and microparticle transport and deposition in an approximate model of the upper tracheobronchial airways. J. Appl. Physiol. 104 (6), 1761–1777.
Zhang, Z., Kleinstreuer, C., Kim, C.S., 2002. Micro-particle transport and deposition in a human oral airway model. J. Aerosol Sci. 33 (12), 1635–1652.